2023

Polyethylene microplastics impede the innate immune response by disrupting the extracellular matrix and signaling transduction

Haipeng Huang

Jiaqi Hou

Yilie Liao

Fangchao Wei

Baoshan Xing

Huang, Haipeng; Hou, Jiaqi; Liao, Yilie; Wei, Fangchao; and Xing, Baoshan, "Polyethylene microplastics impede the innate immune response by disrupting the extracellular matrix and signaling transduction" (2023). *iScience*. 43.
https://doi.org/10.1016/j.isci.2023.107390

iScience

CellPress
OPEN ACCESS

Article

Polyethylene microplastics impede the innate immune response by disrupting the extracellular matrix and signaling transduction

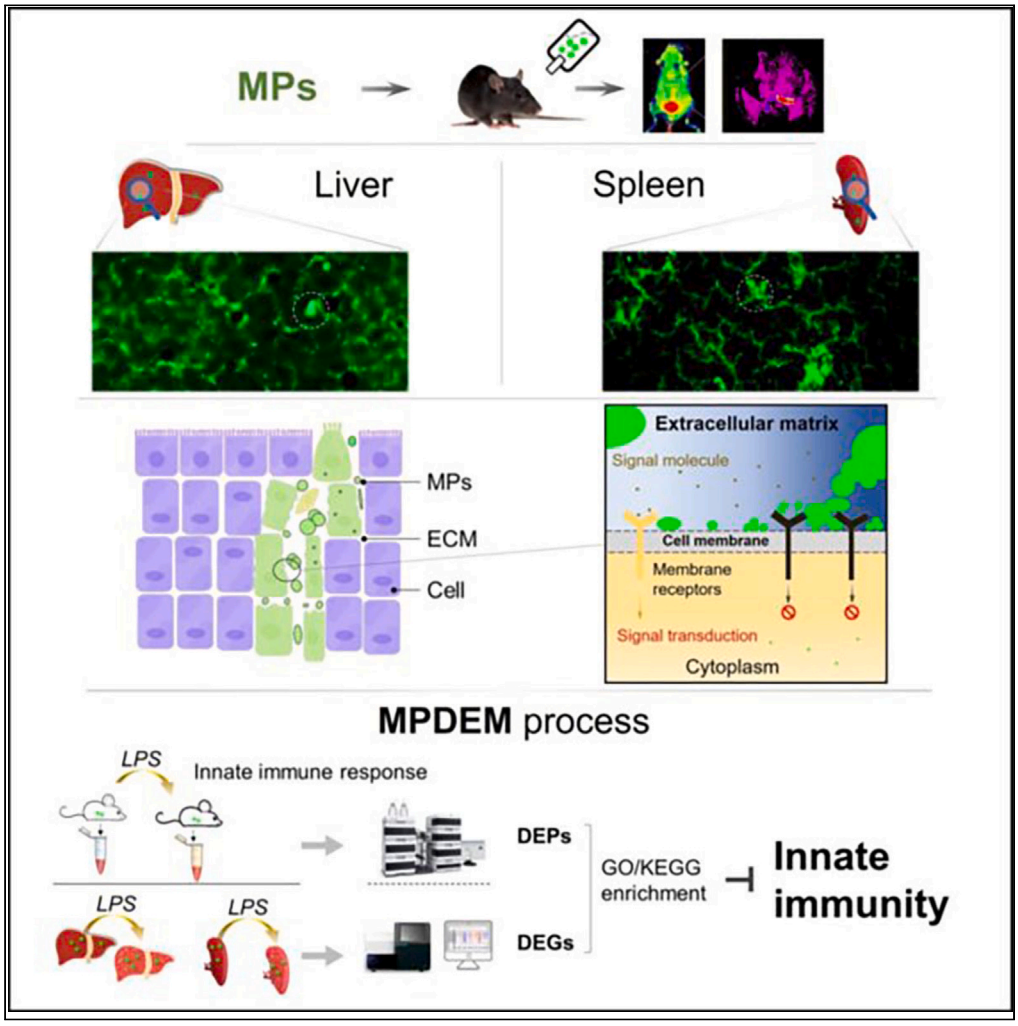

Haipeng Huang, Jiaqi Hou, Yilie Liao, Fangchao Wei, Baoshan Xing

houjiaqi0325@163.com (J.H.)
bx@umass.edu (B.X.)

Highlights

MPs could suppress the innate immune response in mice

Transcriptomic analysis showed impaired ECM function by MP

MPs were abundantly present in the ECM of tissues

MPs inhibited immune response signal transduction by disruption of ECM

Huang et al., iScience *26*, 107390
August 18, 2023
https://doi.org/10.1016/j.isci.2023.107390

iScience

CellPress
OPEN ACCESS

Article

Polyethylene microplastics impede the innate immune response by disrupting the extracellular matrix and signaling transduction

Haipeng Huang,[2,3] Jiaqi Hou,[1,6,*] Yilie Liao,[2] Fangchao Wei,[2,4] and Baoshan Xing[5,*]

SUMMARY

Microplastics (MPs) can accumulate in animal organs. Numerous studies have linked MPs with immune system. However, the impact of MPs on immune response remains unclear. This study examined the innate immune response of mice exposed to 5 μm MPs. In the lipopolysaccharide challenge, mice treated with MPs exhibited lower levels of serum immune factors and activated immune cells. MPs disrupted immune-related receptors and cause dysfunction in cell signal transduction within the liver and spleen. Proteomic analysis revealed that MPs impede the activation of serum immune-related signals. In addition, the tissue section imaging exhibited a significant enrichment of MPs in the extracellular matrix (ECM), consistent with the ECM dysfunction and immune receptor suppression. Therefore, our data suggest excessive MPs accumulation in ECM inhibits cell signaling pathways, thereby suppressing the activation of immune responses. We propose the biotoxicity of MPs is partly through the MP disruption of ECM (MPDEM).

INTRODUCTION

Plastic pollution has emerged as a critical issue with the exponential growth of plastic usage. Currently, there is significant attention being paid to microplastics (MPs), a novel class of environmental pollutants that are chemically stable and can persist in the environment for extended periods.[1,2] Moreover, MPs have the potential to accumulate in organisms,[3–5] posing a threat to both the biosphere and human health.[6,7]

Environmental MPs are inadvertently ingested and accumulate in microorganisms, such as algae and other low-trophic level animals, due to their ubiquitous distribution and diminutive size.[8–10] After deposition in biological tissues, MPs are transferred up the food chain.[11,12] Significant amounts of MPs (mostly <3 μm) have been discovered in the hemolymph of crustaceans in the ocean.[13,14] Additionally, MPs are consistently detected within the digestive tracts of fish.[15] Moreover, substantial quantities of MPs have been found in birds' digestive systems and seabirds can even serve as sensitive indicators for MP pollution levels.[16,17] MPs can be detected in human drinking water and food, particularly seafood.[18–21] Moreover, there is evidence of MP accumulation in various human tissues,[22] including placentas.[23] Therefore, humans and other living organisms face an elevated risk of exposure to and accumulation of MPs.

Numerous studies have demonstrated that exposure to MPs poses a serious threat to the health of organisms.[24] Following exposure of mice or zebrafish to MPs, these particles deposit in multiple tissues. The uptake of micron-scale MPs occurs primarily through gut-associated lymphatic tissue,[25–27] as opposed to nanoscale plastics which are taken up by villus cells via pinocytosis in the gut. These MPs can accumulate in the gut, leading to dysfunction of the gut barrier, dysbiosis of microbiota, and metabolic disorders.[28,29] Additionally, a portion of MPs can be transferred and accumulated in various other tissues. The use of fluorescently labeled MPs aids in tracing their location.[30] The presence of MPs in the liver resulted in the disruption of bile acid metabolism and induction of oxidative stress.[29–31] Transcriptome sequencing and functional analysis revealed that MPs affect various biological processes, including metabolic dysfunction and immune system alterations.[32–36]

The immune system is a complex network of defense responses in advanced vertebrates, including humans, that aids in the repulsion of disease-causing pathogens. Innate immunity, which consists of

[1]State Key Laboratory of Environmental Criteria and Risk Assessment, Chinese Research Academy of Environmental Sciences, Beijing 100012, China

[2]School of Life Science, Tsinghua University, Beijing 100084, China

[3]Institute of Molecular Medicine, College of Future Technology, Peking University, Beijing 100871, China

[4]Department of Pharmacology and Cancer Biology, Duke University, Durham, NC 27708, USA

[5]Stockbridge School of Agriculture, University of Massachusetts, Amherst, MA 01003, USA

[6]Lead contact

*Correspondence: houjiaqi0325@163.com (J.H.), bx@umass.edu (B.X.)

https://doi.org/10.1016/j.isci.2023.107390

nonspecific protective mechanisms, effectively thwarts microorganisms from entering and proliferating within the tissues. The spleen serves as a crucial innate immune organ, while the liver plays a dual role in both metabolism and frontline immunity.[37,38] Upon infection, immediate activation of the liver and spleen occurs. In order to prevent an unbridled exponential growth of viruses and bacteria,[37,38] it is imperative for the host to swiftly eradicate antigens during the initial phase of infection. The promptness of the immune response holds paramount importance during this period. An effective immune response commences with the recognition and capture of antigens, followed by the release of immune cytokines to facilitate immune cell proliferation and differentiation, thereby eliminating pathogens.[39,40] A well-coordinated and efficient immune response aids in eradicating the pathogen during the early stages of infection. The extracellular matrix (ECM) is a complex network composed of various multi-domain macromolecules arranged according to the specific cell or tissue type in which they are located.[41] Cell-ECM interactions occur at specialized, multi-protein adhesion complexes that physically link the ECM to both the cytoskeleton and intracellular signaling pathways.[42,43] The ability of animal cells to perceive and adhere to the ECM plays a crucial role in controlling cell shape, mechanical responsiveness, motility, as well as development and immune response.[41] Thus, a coordinated and orderly immune response also relies on the ECM for signaling transduction.

Through transcriptome sequencing, a study has demonstrated that MP can modulate immune-related signaling pathways in the liver of mice.[33] Moreover, ingestion of MP by zebrafish resulted in the suppression of multiple immune pathways in the gut and damage to immune cells.[32] However, the defense process of the immune system requires intricate regulation. The impact of MPs on immune response remains unclear. Specifically, it is unknown how MPs modulate the innate immune response and whether they affect its speed and strength. These issues remain ambiguous. The objective of this study is to investigate the role of polyethylene MP in the innate immune response through a multi-omics approach, utilizing the classical lipopolysaccharide (LPS) immune challenge infection model and detecting various markers of the immune response at multiple levels for a comprehensive understanding. We conducted whole-transcriptome sequencing and proteomics measurements to investigate the immune response. Additionally, we utilized frozen section imaging technology to accurately detect the fluorescent signal of MPs, revealing specific distribution patterns in organs. By combining these omics analysis results, we proposed a potential mechanism for how MPs modulate biological processes.

RESULTS

MPs inhibit the immune response induced by LPS

Experimental mice were subjected to a 6-week regimen of MPs treatment (Figure 1A). FITC-labeled polyethylene MPs spheres were utilized for mice MPs exposure, and fluorescent signals were also detected inside the spheres (Figure 1B). Initially, we assessed the accumulation of MPs in mice. As depicted in Figure 1C, clear fluorescence signals were observed in mice following exposure to MPs. The signal was distributed throughout the epidermis of the mouse and was particularly concentrated in the urinary bladder. Fluorescent imaging of the liver revealed a significant accumulation of MPs in mice liver compared to the control group (Figure 1D). However, no significant differences were observed in liver weight or triglyceride content during this trial (Figures S1A and S1B).

The LPS challenge is a classic model for studying the innate immune response.[44] In this study, we induced an immune response by injecting LPS. Both groups showed a significant increase in tumor necrosis factor-alpha (TNF-α) and interleukin-6 (IL-6) levels in serum after LPS injection (Figures 1E and 1F). However, mice treated with MPs exhibited significantly lower levels of TNF-α and IL-6 following the LPS challenge. We also quantified the blood monocyte population, which is known to increase in response to innate immunity.[45] The lymphocyte count was reduced following the LPS challenge (Figures 1G and 1H), while the blood monocyte count increased in both groups (Figure 1I). However, the increase in monocytes was significantly suppressed compared to the control group. These results were consistent with cytokine changes observed (Figures 1E and 1F), indicating that mice treated with MPs experienced an inadequate physiological response.

MP modulates multiple signaling pathways in liver

To investigate the impact of MPs on immune response, we conducted whole-transcriptome sequencing in the liver, as it undergoes significant and crucial transcriptional mobilization during an immune response.[46] Specifically, we compared transcriptome data under three conditions: MPs-induced alterations in

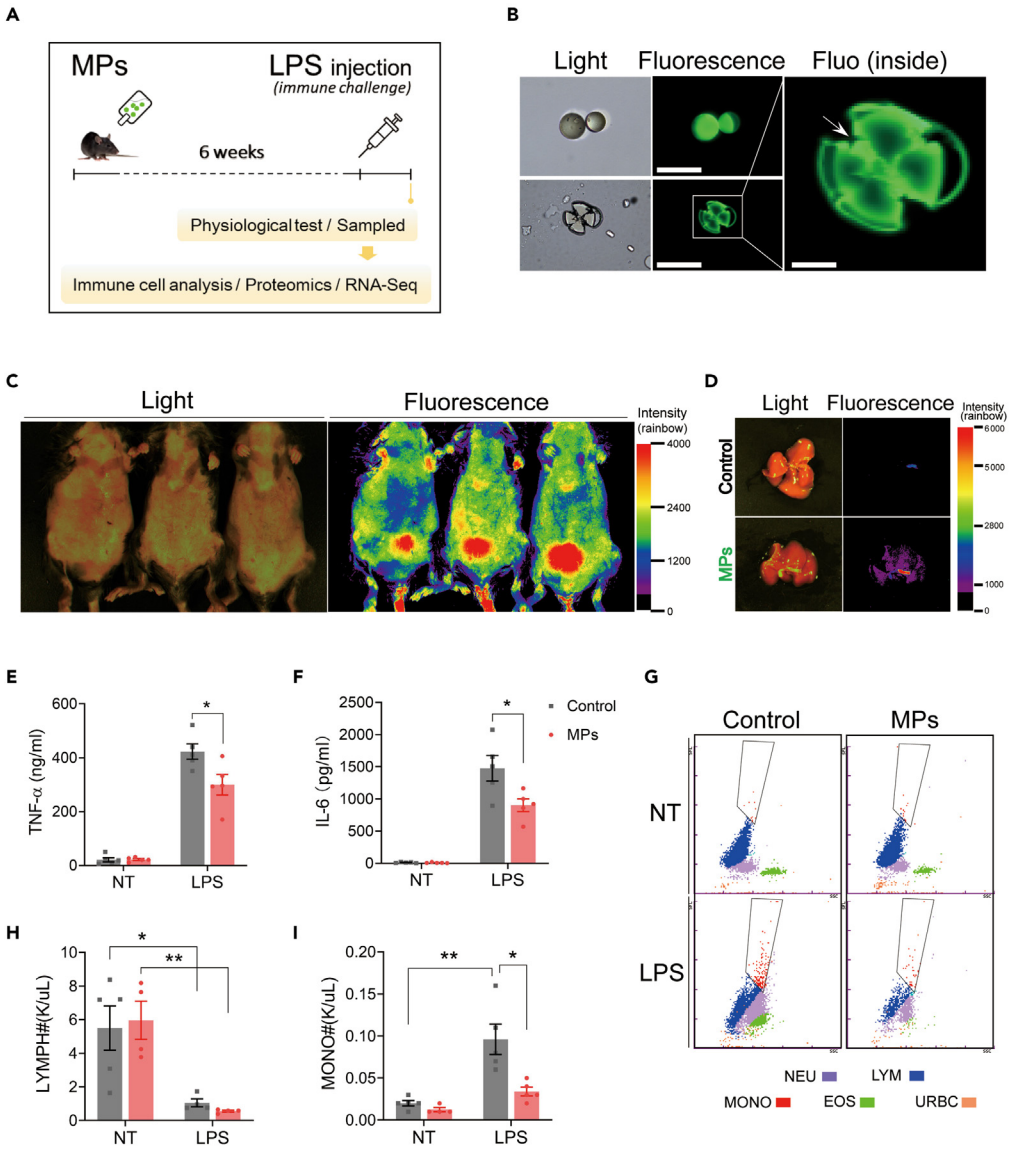

Figure 1. MPs inhibit the immune response induced by LPS

(A) Schematic representation of the MP treatment and subsequent immune challenge with LPS.

(B) Fluorescence images of fluorescently labeled MPs (~5 μm). Scale bars, 10 μm.

(C) Fluorescence images of MPs distribution *in vivo*, mice received MPs (10 μg/mL) for 6 weeks. The rainbow bar represents the relative fluorescence intensity of MPs, the intensity was calculated by normalizing to blank space.

(D) Fluorescence images of the liver.

(E and F) TNF-α and IL-6 levels in serum, before and post LPS challenge.

(G–I) Measurements of cell population in blood by using IDEXX ProCyte Dx (n = 5), before and post LPS challenge and the population of monocyte was highlighted by the box (G), lymphocyte count (H), monocyte count (I). Data are presented as mean ± SEM. *p < 0.05, **p < 0.01. See also Figure S1.

transcriptome, LPS-induced alterations in transcriptome, and the effect of MPs on LPS-induced alterations in transcriptome (Figure 2A).

Firstly, we assess the impact of MPs accumulation on liver function. Control and MPs-treated mice exhibited >93.8% successfully detected reads (Figures S2A and S2B), indicating a comparable transcriptome profile. We identified differentially expressed genes (DEGs); 210 genes were downregulated while 361 genes were up-regulated by MPs exposure (Figure S2C). Among the top 20% DEGs ranked by fold changes, 78% were

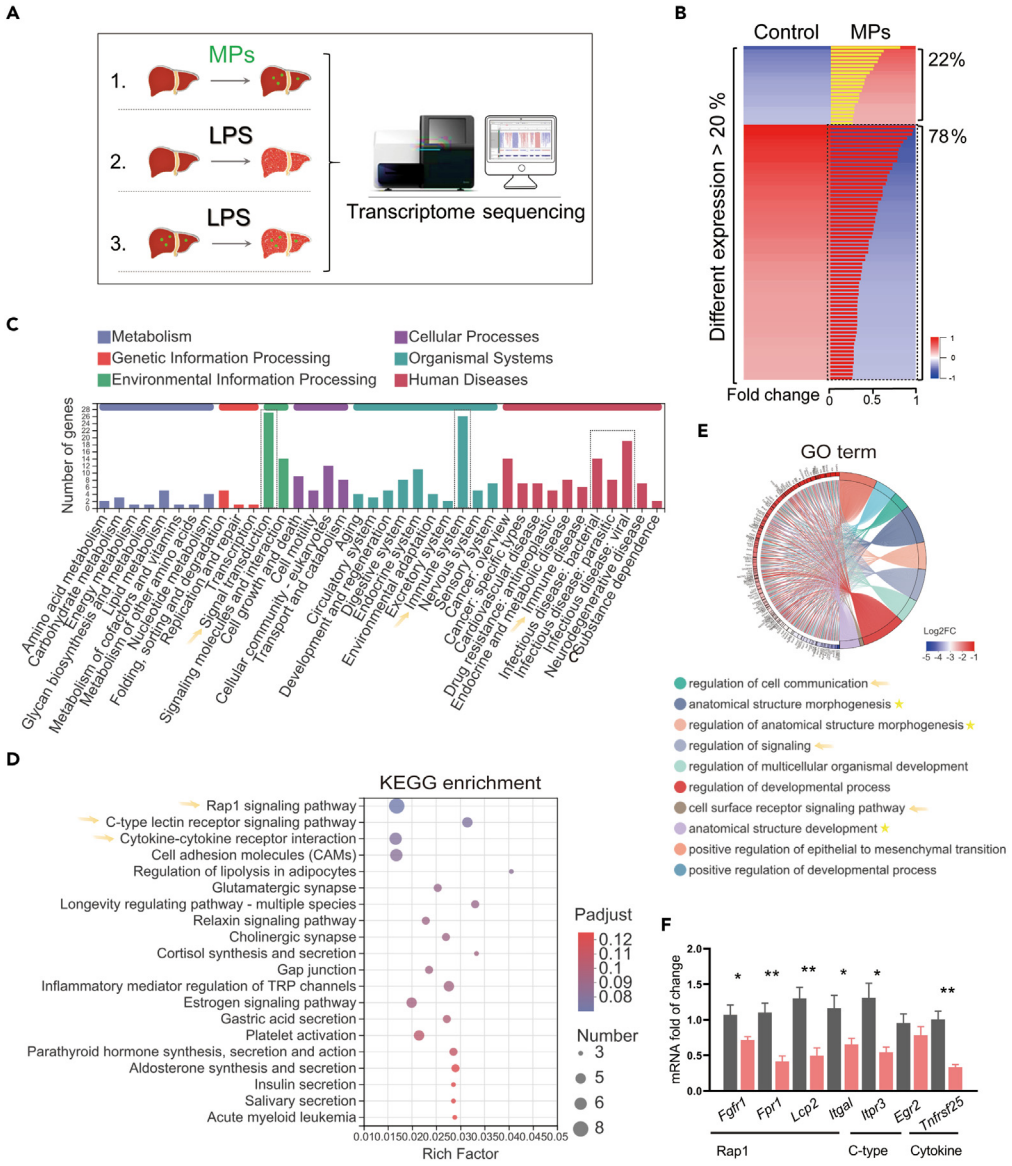

Figure 2. MP modulates multiple signaling pathways in liver

(A) Schematic representation of comparative analysis of hepatic transcriptome data.

(B) The top 20% differentially expressed genes (DEGs) ranked by fold changes, the upregulated DEGs by MPs (yellow bar) and the downregulated DEGs by MPs (red bar).

(C) The functional annotation analysis of downregulated DEGs by MPs, utilizing the KEGG metabolic pathway. Enriched terms of higher significance are marked by dashed boxes and arrows.

(D) KEGG analysis was performed on DEGs downregulated by MPs and the top 20 enriched pathways were shown here. Highly enriched signal transduction-related terms are marked with arrows.

(E) Gene Ontology analysis was performed on DEGs downregulated by MPs and the top 10 enriched pathways were shown here. The signal transduction-related terms that are highly enriched are indicated by arrows, while the structurally relevant terms that are highly enriched are marked with pentagrams.

(F) Transcript levels of representative genes in the top 3 pathways of KEGG analysis, the results normalized to *18S* ribosome RNA (n = 4). Data are presented as mean ± SEM. *p < 0.05, **p < 0.01. See also Figures S2 and S3.

observed to be downregulated by MPs, indicating a global inhibitory effect of MPs on the liver transcriptome. Subsequently, functional annotation analysis of the downregulated DEGs revealed that signal transduction, immune system, and infectious disease were among the most significant terms. They were all closely associated with the regulation of the immune system. More specifically, the top 4 pathways enriched in the KEGG analysis

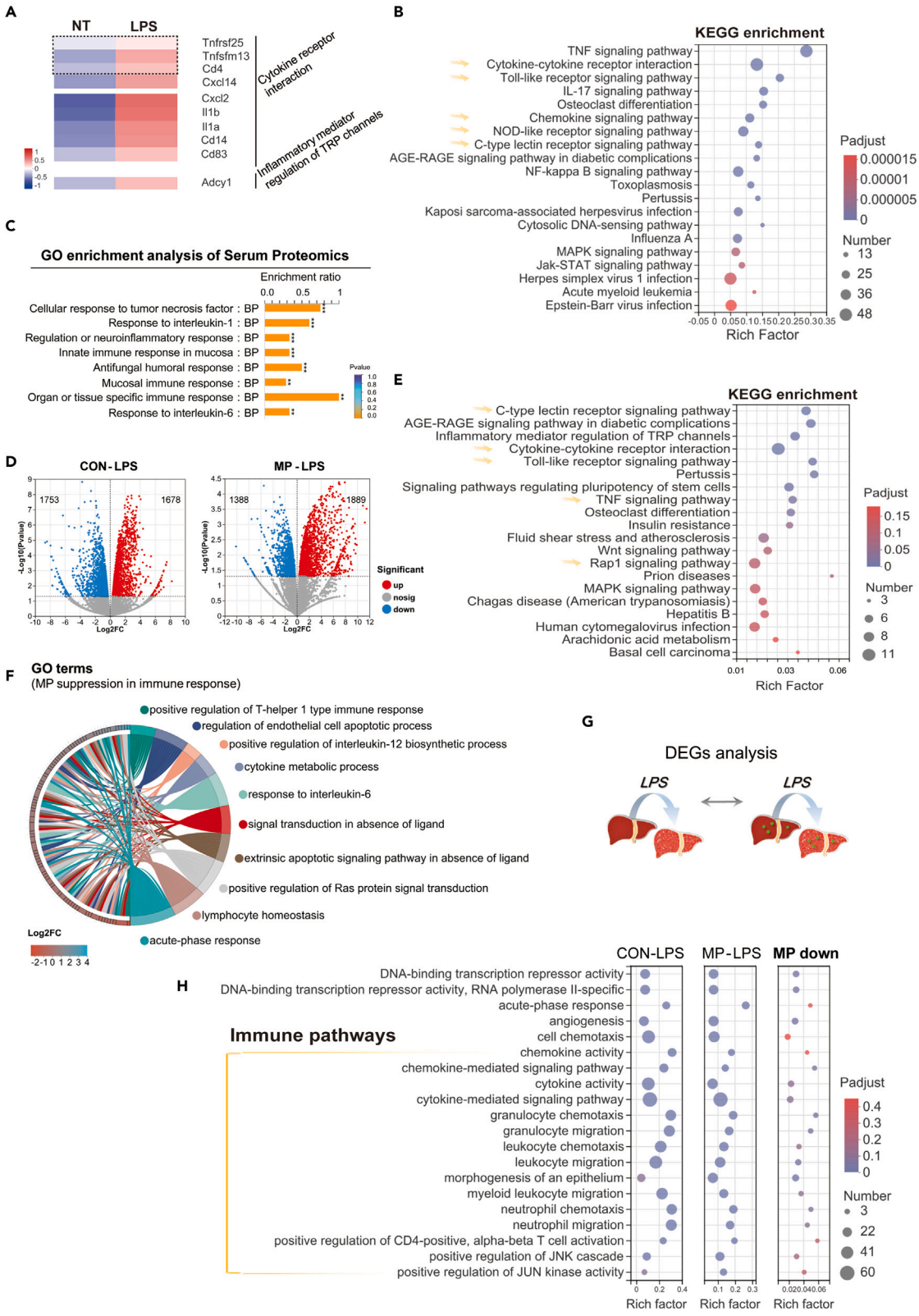
A
NT
LPS
Tnfrsf25
Tnfsfm13
Cd4
Cxcl14
Cxcl2
Il1b
Il1a
Cd14
Cd83
Adcy1
Cytokine receptor interaction
Inflammatory mediator regulation of TRP channels
B
KEGG enrichment
TNF signaling pathway
Cytokine-cytokine receptor interaction
Toll-like receptor signaling pathway
IL-17 signaling pathway
Osteoclast differentiation
Chemokine signaling pathway
NOD-like receptor signaling pathway
C-type lectin receptor signaling pathway
AGE-RAGE signaling pathway in diabetic complications
NF-kappa B signaling pathway
Toxoplasmosis
Pertussis
Kaposi sarcoma-associated herpesvirus infection
Cytosolic DNA-sensing pathway
Influenza A
MAPK signaling pathway
Jak-STAT signaling pathway
Herpes simplex virus 1 infection
Acute myeloid leukemia
Epstein-Barr virus infection
Rich Factor
Padjust
Number
C
GO enrichment analysis of Serum Proteomics
Enrichment ratio
Cellular response to tumor necrosis factor : BP
Response to interleukin-1 : BP
Regulation or neuroinflammatory response : BP
Innate immune response in mucosa : BP
Antifungal humoral response : BP
Mucosal immune response : BP
Organ or tissue specific immune response : BP
Response to interleukin-6 : BP
Pvalue
D
CON - LPS
MP - LPS
1753
1678
1388
1889
-Log10(Pvalue)
Log2FC
Significant
up
nosig
down
E
KEGG enrichment
C-type lectin receptor signaling pathway
AGE-RAGE signaling pathway in diabetic complications
Inflammatory mediator regulation of TRP channels
Cytokine-cytokine receptor interaction
Toll-like receptor signaling pathway
Pertussis
Signaling pathways regulating pluripotency of stem cells
TNF signaling pathway
Osteoclast differentiation
Insulin resistance
Fluid shear stress and atherosclerosis
Wnt signaling pathway
Rap1 signaling pathway
Prion diseases
MAPK signaling pathway
Chagas disease (American trypanosomiasis)
Hepatitis B
Human cytomegalovirus infection
Arachidonic acid metabolism
Basal cell carcinoma
Rich Factor
Padjust
Number
F
GO terms
(MP suppression in immune response)
positive regulation of T-helper 1 type immune response
regulation of endothelial cell apoptotic process
positive regulation of interleukin-12 biosynthetic process
cytokine metabolic process
response to interleukin-6
signal transduction in absence of ligand
extrinsic apoptotic signaling pathway in absence of ligand
positive regulation of Ras protein signal transduction
lymphocyte homeostasis
acute-phase response
Log2FC
G
DEGs analysis
LPS
LPS
H
CON-LPS
MP-LPS
MP down
Immune pathways
DNA-binding transcription repressor activity
DNA-binding transcription repressor activity, RNA polymerase II-specific
acute-phase response
angiogenesis
cell chemotaxis
chemokine activity
chemokine-mediated signaling pathway
cytokine activity
cytokine-mediated signaling pathway
granulocyte chemotaxis
granulocyte migration
leukocyte chemotaxis
leukocyte migration
morphogenesis of an epithelium
myeloid leukocyte migration
neutrophil chemotaxis
neutrophil migration
positive regulation of CD4-positive, alpha-beta T cell activation
positive regulation of JNK cascade
positive regulation of JUN kinase activity
Rich factor
Rich factor
Rich factor
Padjust
Number

Figure 3. MPs inhibit activation of immune signaling pathways during an immune response

(A) A heatmap depicting the expression of genes in representative KEGG pathways in response to LPS, as revealed by sequencing results.

(B) KEGG analysis was performed on DEGs upregulated by LPS of control mice and the top 20 enriched pathways were shown here. Highly enriched receptor mediated immune pathways are marked with arrows.

(C) GO analysis was performed on DEPs upregulated by LPS in serum of control mice and the top 8 enriched pathways were shown here.

(D) Differential expression of hepatic transcriptome pre- and post-LPS challenge.

(E) KEGG analysis was performed on DEGs downregulated by MPs post-LPS challenge, and the top 20 enriched pathways were shown here. Highly enriched receptor mediated immune pathways are marked with arrows.

(F) Gene Ontology analysis was performed on DEGs downregulated by MPs.

(G) A graphical representation of the intergroup comparison strategy for DEGs induced by LPS.

(H) Multi-clusters enrichment of 3 groups: LPS upregulated DEGs in control (cluster 1) (left), LPS upregulated DEGs in MPs group (cluster 2) (middle); MP-inhibited LPS-induced DEG (cluster 3: cluster 1 compared with cluster 2, the downregulated DEGs in cluster 2) (right). The immune-related pathways that are inhibited by MP are demarcated by yellow wireframes. See also Figures S4 and S5.

of the downregulated DEGs were the Rap1,[47] the C-type lectin receptor,[48] the cytokine-cytokine receptor interaction,[49] and the cell adhesion molecules[50] (Figures 2D and S2D). Notably, three pathways were identified as being involved in membrane receptor-activated signal transduction, while one pathway was found to be associated with cellular junctions—all of which are closely linked to the role of ECM. Furthermore, Gene Ontology (GO) enrichment analysis revealed that three out of the top ten biological processes downregulated in DEGs were related to signal transduction, including cell communication, regulation of signaling, and particularly cell surface receptor signaling (Figure 2E). Additionally, the pathways exhibiting the highest levels of GO enrichment were those involved in regulating developmental processes and anatomical structure morphogenesis. Three of the top ten pathways were related to structural regulation, indicating that MPs had a significant impact on tissue architecture. The ECM plays a pivotal role in maintaining tissue structure and regulating cellular signaling pathways. The functions of enriched KEGG pathways were found to be consistent with those of the enriched GO biological processes, indicating a primary role of MP in tissue. Furthermore, RT-qPCR validation revealed that the majority of genes in the top three representative enriched KEGG pathways were strongly inhibited by MPs accumulation (Figure 2F); the qPCR findings are in agreement with the sequencing outcomes of these genes (Figure S3).

MPs inhibit the activation of immune signaling pathways during an immune response

The administration of LPS is a well-established method for inducing an immune response.[44] In this study, we examined the changes in liver transcriptome following the LPS challenge. Our results demonstrate that hepatic transcriptome undergoes significant remodeling upon stimulation with LPS. The principal component analysis revealed a clear separation between the LPS-treated groups and the control group (Figure S4). PC2 was initially the primary factor distinguishing between control and MPs-treated groups, but this distinction disappeared after LPS injection (Figure S4). PC1 was the dominant factor separating pre-LPS from post-LPS groups. Even with MP treatment, mice clustered similarly to non-MP-treated mice following LPS injection.

Moreover, the upregulation of *Tnfrsf25*, *Tnfsf13*, and *Cd4* induced by LPS (as shown in Figure 3A) was suppressed by MPs treatment (as demonstrated in Figure 2C). Notably, even under non-infection conditions, MPs were found to modulate the cytokine-cytokine receptor pathway (as depicted in Figure 2D). Among the enriched pathways associated with LPS-induced DEGs, a majority of them were immune related (Figure 3B). Furthermore, most of the top activated pathways involved cell membrane receptors such as the TNF signaling pathway, cytokine-cytokine receptor pathway, and Toll-like receptor[51] signaling pathway. We conducted liquid chromatography-tandem mass spectrometry analysis of serum samples collected before and after the LPS challenge. As anticipated, numerous immune-related processes were significantly activated (Figure 3C), which is consistent with the activation of immune signaling in the liver. These findings suggest a successful induction of systemic immune response.

We then conducted a comprehensive analysis to comprehend the impact of MPs on the LPS-induced immune response process (Figure 2A). We hypothesized that MPs could suppress the immune response by affecting membrane receptor function. In control mice, LPS upregulated 984 genes, while exposure to MPs resulted in an upregulation of 1033 genes (Figure 3D). Afterward, we conducted a comparison of the transcriptome following the LPS challenge. Notably, MPs exhibited an enrichment of suppressed DEGs in C-type lectin receptor signaling, cytokine-cytokine receptor interaction, and Rap1 signaling pathways under both normal and immune challenge conditions (Figure 3E). Conversely, our findings indicated that several major immune pathways were inhibited by MPs post-LPS challenge, including the transient receptor potential channels and Toll-like

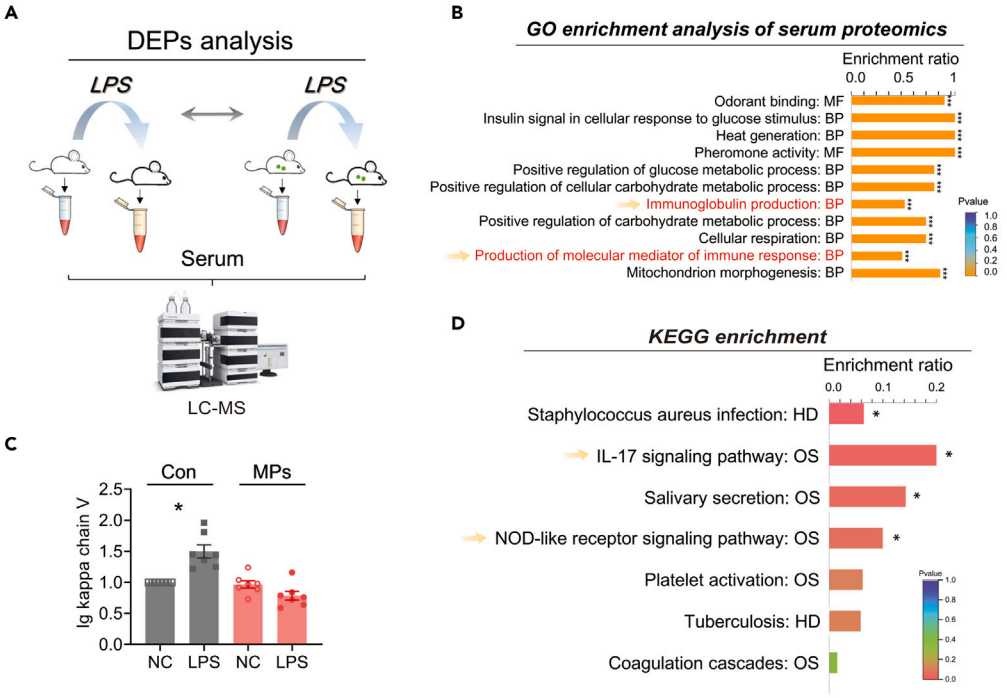

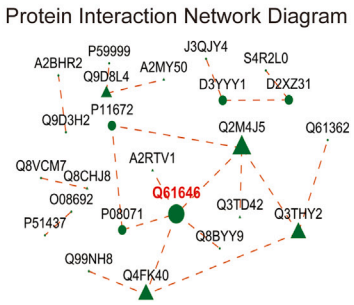

F

MS Fragment ID	Gene name	Subcellular Location	Biological Process
Q61646	*Serpina3b*	Extracelluar space	Inflammatory response
Q61646	*Serpina3i*	Extracelluar space	Inflammatory response
Q61646	*Apoe*	Extracelluar space	Anatomical structure development
Q61646	*Lcn11*	Extracelluar space	Cell wall
Q61646	*Ltf*	Extracelluar space	Innate immune response
Q61646	*Mmp9*	Extracelluar space	Immune process/signalling

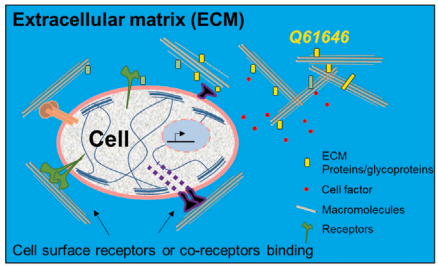

Figure 4. Detection of immune activation in serum under immune challenge

(A) Schematic illustration of LC-MS/MS analysis design for serum proteomics.

(B) GO analysis was performed on DEPs downregulated by MPs post-LPS challenge, and the top 11 enriched pathways were shown here. Highly enriched immune pathways are marked with arrows.

(C) Statistical analysis of immunoglobulin Ig kappa chain V fragments in MS, data normalized to the corresponding fragment in control.

(D) KEGG functional annotation analysis on DEPs downregulated by MPs post-LPS challenge, the top 7 enriched pathways were shown here. Highly enriched receptor mediated immune pathways are marked with arrows.

(E) Using the STRING database, we established a protein interaction network diagram through sequence alignment analysis: nodes represent proteins and edges denote interactions between two proteins. The size of the node is proportional to its degree, which reflects the number of connections it has with other nodes in the network. A larger node

Figure 4. *Continued*
indicates a higher degree of connectivity and thus greater importance within the network. Q61646 is highlighted in red for emphasis.
(F) Proteins corresponding to fragment Q61646. Their corresponding gene names, subcellular locations, and biological processes involved. The proteins information is sourced from the UNIPROT database (https://www.uniprot.org/).
(G) A schematic diagram illustrating the potential subcellular localization of Q61646. Data are presented as mean ± SEM. *p < 0.05. See also Figure S6.

receptor pathway (Figure 3E). Furthermore, GO enrichment analysis revealed that the most enriched term was the acute-phase response (Figure 3F). Numerous immune-related terms were enriched, all of which were suppressed by MP following LPS induction. Additionally, a comparison of the gene clusters reveals that approximately 10% of the specific DEGs upregulated by LPS in control were overlapped with the inhibited DEGs by MPs during the immune challenge (Figure S4C). These findings suggest that MPs diminish the functional upregulation of immune response genes and simultaneously suppress these immune pathways along with cell membrane receptors pathways during the LPS challenge.

To investigate transcriptional mobilization in the immune response, we conducted functional annotation of multiple gene clusters for LPS upregulated DEGs (Figure 3G). During the activation process of immune signaling, fewer genes were annotated in terms of the immune system and response to stimulus in the MPs group (Figure S5). We further performed multiple gene cluster enrichment analyses. The immunological pathway, encompassing chemokine and cytokine activities as well as neutrophil migration, exhibited lower enrichment significance and a reduced gene count in the MPs group (Figure 3H). These findings collectively suggest that MPs induce receptor dysfunction, thereby suppressing immune signaling activation during the LPS challenge.

Detection of immune activation in serum under immune challenge

To provide a more comprehensive understanding of the role of MPs in immune response, we conducted a comparison between changes in serum proteome of control and MPs-treated groups during the LPS challenge (Figure 4A). Firstly, we identified differentially expressed proteins (DEPs) in the LPS-treated group. Then, we compared the downregulated and upregulated DEPs by MPs during the immune activation of serum. There were 141 DEPs upregulated by MPs, and 159 DEPs downregulated by MPs. Multiple immune processes, BP terms for IGP, and PMIR enriched in the LPS challenge group were all repressed by MPs (Figure 4B). Additionally, the DEPs upregulated by MPs did not include any immune-related biological processes, as shown in Figure S6. We summarized the typical immunoglobulin levels measured in MS and found that LPS induced significant elevations of immunoglobulin in control mice, but no induction was observed in mice treated with MPs, as depicted in Figure 4C. Importantly, KEGG enrichment analysis revealed that pathways related to IL-17 and NOD-like receptor signaling were inhibited by MPs treatment (Figure 4D). It has been reported that the activation of IL-17 signaling pathway is triggered by bacterial or viral infection, and the secretion of IL-17 requires stimulation of $CD4^+$ T cells by IL-6.[52] Therefore, the inhibition of IL-17 was consistent with our observation of reduced levels of IL-6 in the serum of MPs-treated mice (Figure 1F). Moreover, NOD-like receptor activation necessitates IL-1β which is secreted by activated macrophages.[53] The suppression of NOD signaling also aligns with the decreased monocyte level observed in MPs-treated mice.

We then constructed a protein interaction network for the set of proteins inhibited by MP in the immune response. Fragment Q61646 secured the most crucial position in the network (Figure 4E). By comparative analysis of sequence Q61646, we predicted six proteins that were all localized in the ECM, 67% of which were associated with immune response (Figures 4F and 4G). This suggested that MP may regulate immune suppression by acting on ECM proteins. Furthermore, this finding was in line with the liver transcriptome data that suggested MP disrupts tissue architecture and signaling pathways by impacting the ECM (Figure 2F).

MP deposited more in the ECM in liver

Our findings suggest that MPs may suppress immune signaling activation by inducing dysfunction of membrane receptors. Subsequently, we aimed to investigate the mechanism underlying the inhibitory effect of deposited MPs on signal transduction mediated by membrane receptors. Due to the impact of MPs on biological processes related to cell structure (as shown in Figure 2E), we investigated whether there were any changes in cell morphology. In liver sections stained with H&E and containing accumulated MPs, we observed abnormal and irregular hepatocyte morphology (as depicted in Figure 5A). Additionally, flow cytometry analysis revealed a wider distribution of hepatocyte sizes (Figure 5B). Hepatocyte morphology

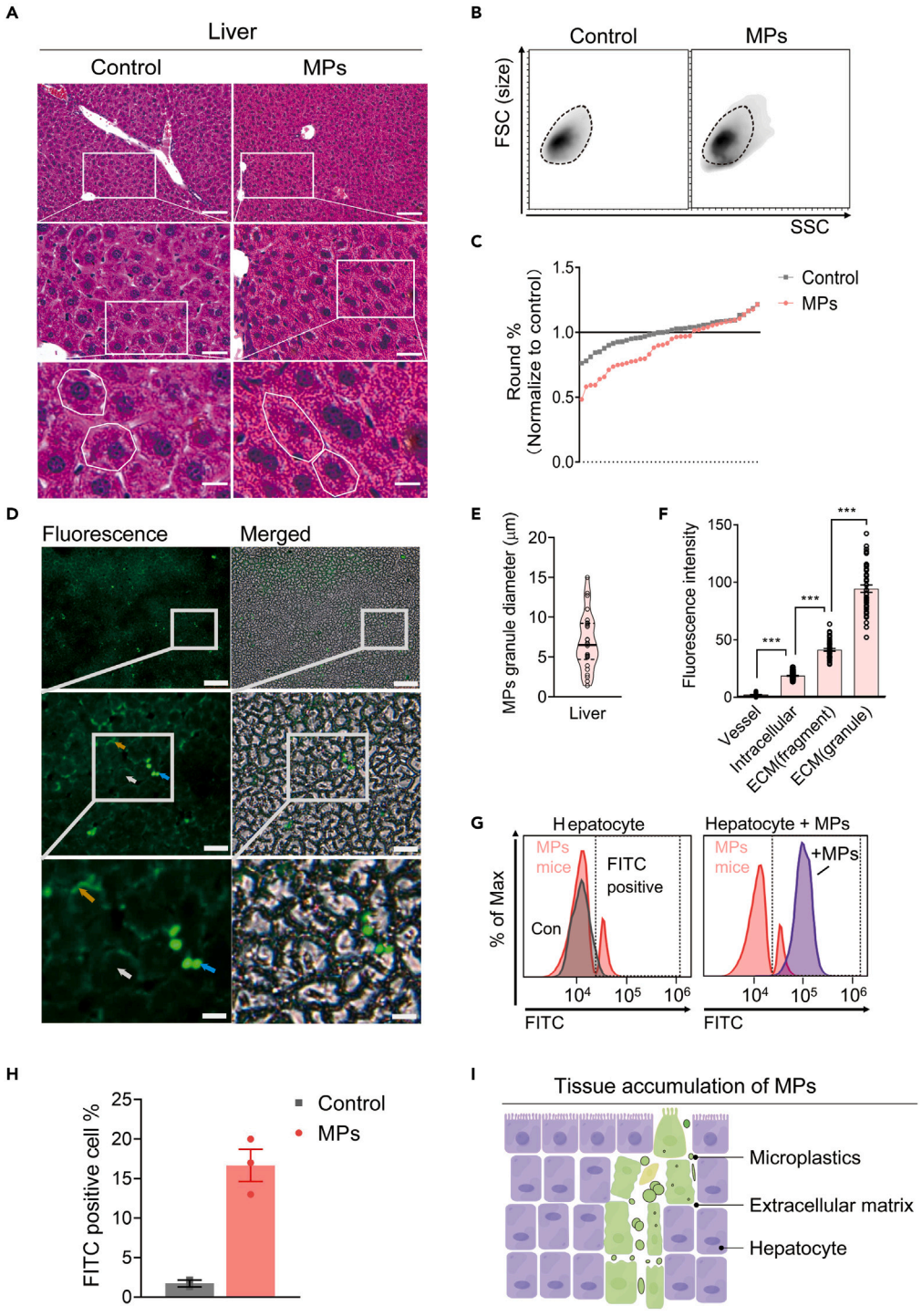

Figure 5. MP deposited more in the ECM in liver

(A) H&E staining of liver sections, typical hepatocyte was marked by a circle. The scale bars from top to bottom represent 75, 25, and 10 μm respectively.

(B) Distribution of hepatocyte size.

(C) Round ratio of hepatocyte was calculated by ImageJ (n = 40), the results normalized to the mean value of control.

(D) Fluorescence images of MPs in frozen sections of liver, accumulated MPs were respectively marked with white arrows (intracellular), orange arrows (ECM-fragment), and blue arrows (ECM-granule). Scale bars from up to bottom, 75, 25, and 10 μm.

Figure 5. *Continued*
(E) Measurement of the diameter of MP granules.
(F) Fluorescence intensity measurements of MPs in liver frozen sections.
(G) Hepatocytes containing MPs were measured by flow cytometry, with positive cells for MPs being highlighted.
(H) The percentage of MPs signaling positive cells was quantified (n = 2 for control and n = 3 for MPs treatment).
(I) Proposed model for hepatic accumulation of MPs. Data are presented as mean ± SEM. *p < 0.05, **p < 0.01, and ***p < 0.001. See also Figures S7–S9.

exhibited higher heterogeneity in the liver with deposited MPs (Figure 5C). These findings were consistent with the cell structure defects observed in bioinformatics analysis (Figure 2E). Subsequently, we conducted a more detailed investigation into the distribution of MPs within the liver. To obtain more *in situ* signals, frozen section imaging was utilized to detect MP signals and minimize the loss of fluorescence signal during chemical treatment. There were distinct characteristics observed in the accumulation of MPs (Figure 5D). Based on the distribution pattern of fluorescence signals, they could be classified into intracellular localization, ECM fragments, and ECM granules (Figures 5D and S7A). The diameter of MP granules deposited in the liver ranged from approximately 2 to 13 μm, with a median diameter of about 5 μm (Figures 5E and S7B). The blood vessel was considered as a negative control, where only minimal fluorescence signal was detected (Figure 5F). The results revealed a significantly higher ECM signal of MPs, which were accumulated in the ECM at 2–4 times the intracellular level (Figures 5F, S7C, and S8A). This suggests that there is more MPs accumulation in the ECM. Furthermore, the fluorescence intensity of ECM-MPs exhibited greater heterogeneity than that of intracellular MPs (Figure S8B), indicating varying degrees of MP aggregation within the ECM. Besides, we sorted hepatocytes containing MPs to validate our findings. Only a small number of hepatocytes exhibited positive fluorescence for MPs (Figure 5G), and the intracellular fluorescence intensity was significantly lower than that observed in the group with exogenous MPs addition. Approximately 15% of hepatocytes contained MPs, indicating that intracellular storage was not the primary site for MP accumulation (Figure 5H). Additionally, certain ECM MPs were observed to co-localize with apoptotic cells in Figure S7D. However, no significant alteration was detected in the liver's apoptosis rate as shown in Figure S9. These findings support our observations that most MPs are deposited within the ECM rather than accumulating intracellular (Figure 5D).

We observed a regular distribution of MPs in the tissue, primarily deposited within the ECM as aggregated particles and distributed throughout the tissue section (Figure 5I). Additionally, cells adhered to the ECM via transmembrane receptors; ECM could modulate membrane receptor signaling and downstream gene expression to regulate cellular processes.[54–57] Thus, these data suggested MP affected signal transduction through MP disruption of the ECM (MPDEM), in which the accumulation of ECM-MPs leads to inert hindrances occupying the ECM, resulting in inevitable changes to multiple functions of the ECM.

MPs deposition of ECM hinders immune signaling pathways in the spleen

We investigated whether MPs could exert an impact on the function of other tissues via a similar MPDEM mechanism. Our analysis revealed that in the spleen, another major immune organ, MPs exhibited three distinct distribution patterns: intracellular localization, ECM fragmentation, and ECM granulation (Figure 6A). The diameter of the deposited MPs granules in the spleen ranged from 1 to 17 μm, which was similar to that observed in the liver (Figure 6B). Furthermore, the intensity of ECM-MPs was significantly higher than that of intracellular MPs (Figure 6C). Similar to our findings in the liver, we also observed an abnormal distribution of cells and excessive leukocyte infiltration in the spleen with MP accumulation (Figure 6D). Furthermore, we conducted transcriptome sequencing of the spleen during the LPS challenge (Figure 6E). Treatment with MPs had significant regulatory effects on the immune challenge-induced transcriptome change of the spleen (Figure 6F). Additionally, comparison of control and MPs-treated spleens revealed consistent KEGG enrichment results with those obtained from liver samples. Notably, downregulated DEGs by MPs in the spleen were highly enriched in receptor signaling pathways, particularly cytokine-cytokine receptor interactions (Figures 6G, 2D and 3B). Furthermore, MPs were found to inhibit B cell receptor signaling as well as other classical immune signaling and immune cell activation pathways (Figure 6G). These findings suggest that ECM-deposited MPs have an impact on cellular signal transduction and suppress the immune response in the spleen. This suggests that the MPDEM process is not limited to the liver and has a broad *in vivo* effect. We have proposed a model illustrating how MPs modulate cell signal transduction in organs (Figure 6I). As receptor activation is essential for immune response (Figures 3B and 4B),[49,58] ECM-deposited MPs suppress receptor-activated immune signaling, resulting in decreased immunity in mice.

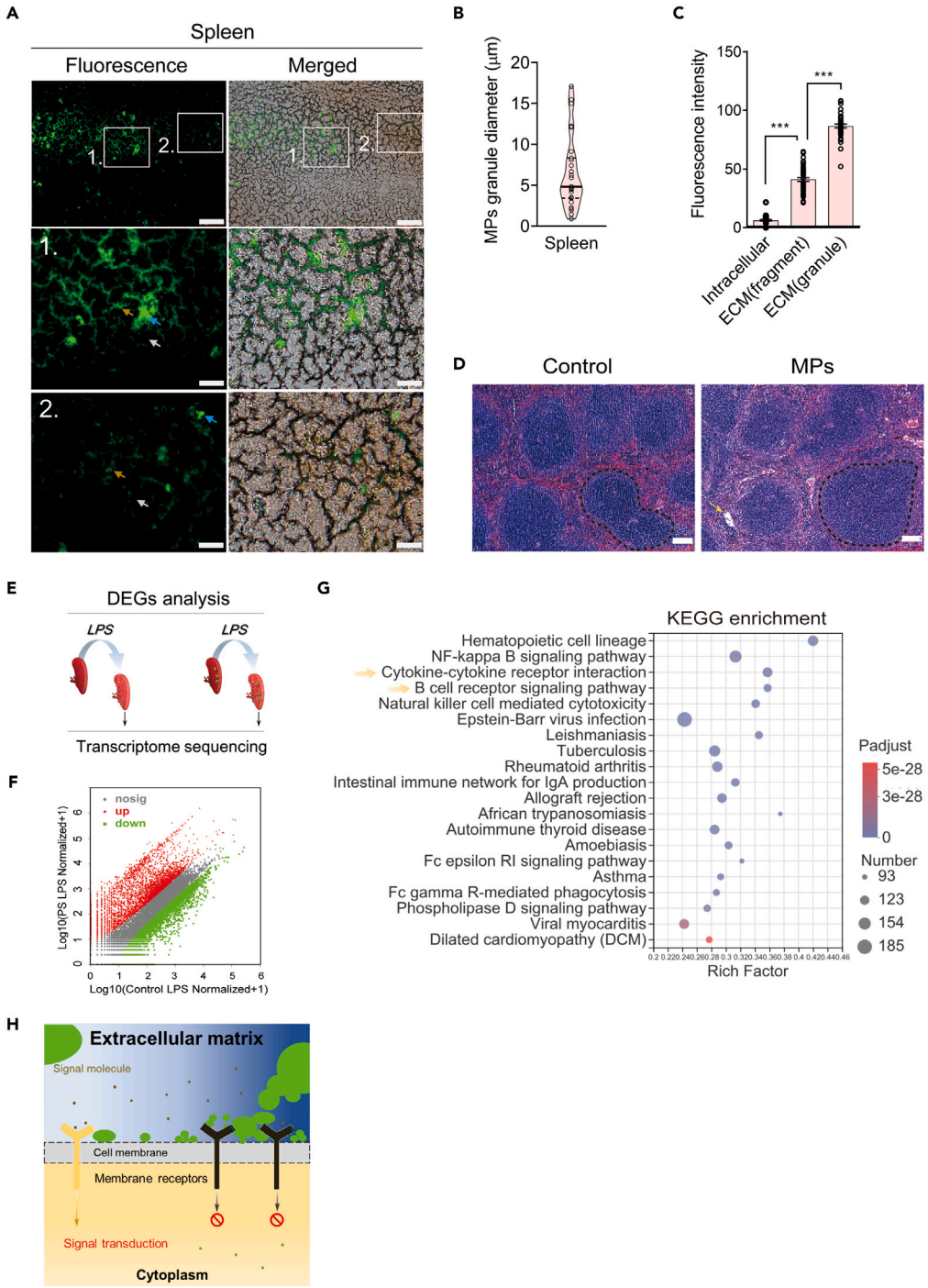

Figure 6. MPs deposition of ECM hinders immune signaling pathways in the spleen

(A) Fluorescence images of MPs in frozen spleen sections were annotated with white arrows for intracellular MPs, orange arrows for ECM fragments, and blue arrows for ECM granules. The scale bars were set at 75 μm for the upper images and 25 μm for the zoom-in images (1 and 2).

(B) Measurement of the diameter of MP granules.

(C) Fluorescence intensity measurements of MPs in spleen frozen sections.

(D) H&E staining of spleen sections, typical cell was marked by a circle. Scale bars, 100 μm.

(E) Schematic representation of spleen tissue samples utilized for transcriptome sequencing.

Figure 6. *Continued*

(F) Scatterplot depicting DEGs in spleen transcriptome sequencing results, with upregulated DEGs highlighted in red and downregulated DEGs in green by MPs.

(G) KEGG analysis was performed on DEGs downregulated by MPs in spleen post-LPS challenge, and the top 20 enriched pathways were shown here. Highly enriched receptor mediated immune pathways are marked with arrows.

(H) Proposed model of MP disruption extracellular matrix (MPDEM) function in organs. Data are presented as mean ± SEM. ***p < 0.001.

DISCUSSION

As the severity of MP pollution continues to increase, more and more studies are being conducted to explore and comprehend the detrimental effects of MPs on human health. Our findings indicate that MPDEM plays a crucial role in immune response dysfunction, which was observed in both liver and spleen tissues, suggesting its conservation across multiple organs. The conservative action of MP within tissues can be attributed to its physical properties, which include difficulty in biodegradation and a specific size that leads to enrichment in the ECM of organs. However, this constant accumulation of MP in the ECM may impair its function as a support structure for cells, as evidenced by our observation of irregular intra-organ structures in the liver and spleen that correlated with MP presence. ECM-MP has the ability to directly interact with the cell membrane. The presence of a significant amount of MP in the ECM can also impact other functions of the ECM, such as cellular communication and signal transduction regulation. We propose that polyethylene MP utilizes its properties to disrupt tissue function through the process of MPDEM.

MPs in organs have been shown to disrupt various biological processes, such as metabolism, cell growth and death, genetic information processing, and the immune system. In this study, we focused on innate immunity and investigated how MPs induce dysfunction in the immune response. Genetic or pharmacological inhibition of immune receptors can lead to suppression of the immune response, highlighting the importance of signal transduction in this process.[58] The immune system's reliance on signal transduction for rapid activation is a crucial characteristic, which has provided us with a unique research perspective to investigate the role of MP in physiological processes that heavily rely on signal transduction. Our data indicate that signal transduction is suppressed in mice treated with MPs (Figures 2D and 3E), and this inhibition has a significant impact, particularly on the immune response. Additionally, we hypothesize that MPs may also play a role in other physiological processes requiring rapid signal transduction, such as hormone secretion and neural signal regulation.

Moreover, the endocytic capacity of cells is a crucial factor in the MPDEM process. Different organs with distinct functions often exhibit varying levels of cellular endocytosis.[59] Enhanced phagocytosis would enable cells to engulf MP rather than allowing its deposition in the ECM. On the other hand, when the size of MP is small enough, such as nanoscale plastic (<280 nm),[35] they can be easily endocytosed by most types of cells and thus tend to accumulate intracellularly rather than depositing in the ECM. Therefore, the MPDEM process is influenced by both cell type and plastic size.

In conclusion, we investigated the impact of MP on immune response in mice and its underlying mechanisms using an immunological induction model. Our findings suggest that MP-mediated regulation of cellular signaling transduction can significantly influence tissue function. In addition to discussing the MPDEM process, we also highlighted the non-signal-induced effects (i.e., without LPS) of MP on tissue and cell function. For example, the KEGG analysis of suppressed DEGs by MP revealed an enrichment in the pathway of cell adhesion molecules (Figure 2D). This suggests that MP directly affects the ECM and may impact other biological processes such as tissue stem cell viability, cell differentiation, growth factor regulation, and even cancer. Our focus in this study was to elucidate the role of MP in signaling transduction within tissue. However, the impact of MP on primary tissue disease through its interaction with ECM remains uncertain. Will it promote or inhibit the progression of diseases such as cancer and neurodegenerative disorders? These questions remain inconclusive. For instance, whether MP will facilitate or impede tumor growth in light of the MPDEM process yet requires experimental validation. Therefore, further attention and research are imperative to explore this area comprehensively.

Limitations of the study

While this study has demonstrated that the ingestion of 5 μm MPs results in the accumulation of significant amounts of MP debris within the ECM of both liver and spleen, it remains unclear whether this phenomenon is applicable to other sizes or nanoscale MPs. Moreover, only sections of liver and spleen were examined in this study, leaving the extent and pattern of MP accumulation in other tissues unclear. Due to the specificity

of organ function, the role of ECM varies across different tissues and biological processes. Therefore, further evidence is needed to determine whether MP's effect on cell signaling is consistent across other tissues.

STAR★METHODS

Detailed methods are provided in the online version of this paper and include the following:

- KEY RESOURCES TABLE
- RESOURCE AVAILABILITY
  - Lead contact
  - Materials availability
  - Data and code availability
- EXPERIMENTAL MODEL AND STUDY PARTICIPANT DETAILS
  - Animal and MPs treatment
- METHOD DETAILS
  - Mice immune challenge
  - Histological analysis
  - Primary hepatocyte isolation and FACS flow cytometry analysis
  - Quantitative reverse transcribed polymerase chain reaction (qRT-PCR)
  - RNA extraction and library preparation
  - Differential gene expression analysis and functional enrichment
  - Serum extraction and proteomic analysis
  - Hematological analysis
  - Serum cytokine measurement
- QUANTIFICATION AND STATISTICAL ANALYSIS

SUPPLEMENTAL INFORMATION

Supplemental information can be found online at https://doi.org/10.1016/j.isci.2023.107390.

ACKNOWLEDGMENTS

We thank Zai Chang from Tsinghua Model Animal Center for mouse husbandry. We thank Suneng Fu for sharing equipment and reagents. This work was supported by the National Key R&D Program of China (No. 2020YFD1100301) and the National Natural Science Foundation of China (No. 51908524).

AUTHOR CONTRIBUTIONS

H.H., J.H., and B.X. conceived and designed this project. H.H. performed most experiments from cell isolation and culture, flow cytometry, tissue section observations, RNA sequencing analysis, and animal studies; Y.L. assisted in RNA sequencing analysis. F.W., J.H., and B.X. supervised the work. H.H. and J.H. wrote the manuscript.

DECLARATION OF INTERESTS

The authors declare no competing interests.

Received: August 7, 2022
Revised: June 1, 2023
Accepted: July 10, 2023
Published: July 13, 2023

REFERENCES

1. Moore, C.J. (2008). Synthetic polymers in the marine environment: a rapidly increasing, long-term threat. Environ. Res. *108*, 131–139. https://doi.org/10.1016/j.envres.2008.07.025.

2. Barnes, D.K.A., Galgani, F., Thompson, R.C., and Barlaz, M. (2009). Accumulation and fragmentation of plastic debris in global environments. Philos. Trans. R. Soc. Lond. B Biol. Sci. *364*, 1985–1998. https://doi.org/10.1098/rstb.2008.0205.

3. Auta, H.S., Emenike, C.U., and Fauziah, S.H. (2017). Distribution and importance of microplastics in the marine environment: a review of the sources, fate, effects, and potential solutions. Environ. Int. *102*, 165–176. https://doi.org/10.1016/j.envint.2017.02.013.

4. Wright, S.L., and Kelly, F.J. (2017). Plastic and human health: a micro issue? Environ. Sci. Technol. *51*, 6634–6647. https://doi.org/10.1021/acs.est.7b00423.

5. Sun, X.D., Yuan, X.Z., Jia, Y., Feng, L.J., Zhu, F.P., Dong, S.S., Liu, J., Kong, X., Tian, H., Duan, J.L., et al. (2020). Differentially charged nanoplastics demonstrate distinct

accumulation in Arabidopsis thaliana. Nat. Nanotechnol. *15*, 755–760. https://doi.org/10.1038/s41565-020-0707-4.

6. Bastyans, S., Jackson, S., and Fejer, G. (2022). Micro and nano-plastics, a threat to human health? Emerg. Top. Life Sci. *6*, 411–422. https://doi.org/10.1042/ETLS20220024.

7. Amaral-Zettler, L.A., Zettler, E.R., Slikas, B., Boyd, G.D., Melvin, D.W., Morrall, C.E., Proskurowski, G., and Mincer, T.J. (2015). The biogeography of the Plastisphere: implications for policy. Front. Ecol. Environ. *13*, 541–546. https://doi.org/10.1890/150017.

8. Hämer, J., Gutow, L., Köhler, A., and Saborowski, R. (2014). Fate of microplastics in the marine isopod Idotea emarginata. Environ. Sci. Technol. *48*, 13451–13458. https://doi.org/10.1021/es501385y.

9. Dawson, A., Huston, W., Kawaguchi, S., King, C., Cropp, R., Wild, S., Eisenmann, P., Townsend, K., and Bengtson Nash, S. (2018). Uptake and depuration kinetics influence microplastic bioaccumulation and toxicity in Antarctic Krill (Euphausia superba). Environ. Sci. Technol. *52*, 3195–3201. https://doi.org/10.1021/acs.est.7b05759.

10. Steer, M., Cole, M., Thompson, R.C., and Lindeque, P.K. (2017). Microplastic ingestion in fish larvae in the Western english channel. Environ. Pollut. *226*, 250–259. https://doi.org/10.1016/j.envpol.2017.03.062.

11. Miranda, D.d.A., and de Carvalho-Souza, G.F. (2016). Are we eating plastic-ingesting fish? Mar. Pollut. Bull. *103*, 109–114. https://doi.org/10.1016/j.marpolbul.2015.12.035.

12. Ivar do Sul, J.A., and Costa, M.F. (2014). The present and future of microplastic pollution in the marine environment. Environ. Pollut. *185*, 352–364. https://doi.org/10.1016/j.envpol.2013.10.036.

13. Thompson, R.C., Olsen, Y., Mitchell, R.P., Davis, A., Rowland, S.J., John, A.W.G., McGonigle, D., and Russell, A.E. (2004). Lost at sea: where is all the plastic? Science *304*, 838. https://doi.org/10.1126/science.1094559.

14. von Moos, N., Burkhardt-Holm, P., and Köhler, A. (2012). Uptake and effects of microplastics on cells and tissue of the blue mussel Mytilus edulis L. after an experimental exposure. Environ. Sci. Technol. *46*, 11327–11335. https://doi.org/10.1021/es302332w.

15. van Noord, J.E. (2013). Diet of five species of the family Myctophidae caught off the Mariana Islands. Ichthyol. Res. *2013*, 89–92. https://doi.org/10.1007/s10228-012-0315-x.

16. Ryan, P.G. (2008). Seabirds indicate changes in the composition of plastic litter in the Atlantic and south-western Indian Oceans. Mar. Pollut. Bull. *56*, 1406–1409. https://doi.org/10.1016/j.marpolbul.2008.05.004.

17. Zhao, S., Zhu, L., and Li, D. (2016). Microscopic anthropogenic litter in terrestrial birds from Shanghai, China: not only plastics but also natural fibers. Sci. Total Environ. *550*, 1110–1115. https://doi.org/10.1016/j.scitotenv.2016.01.112.

18. Barboza, L.G.A., Dick Vethaak, A., Lavorante, B.R.B.O., Lundebye, A.K., and Guilhermino, L. (2018). Marine microplastic debris: An emerging issue for food security, food safety and human health. Mar. Pollut. Bull. *133*, 336–348. https://doi.org/10.1016/j.marpolbul.2018.05.047.

19. Karami, A., Golieskardi, A., Keong Choo, C., Larat, V., Galloway, T.S., and Salamatinia, B. (2017). The presence of microplastics in commercial salts from different countries. Sci. Rep. *7*, 46173. https://doi.org/10.1038/srep46173.

20. Kosuth, M., Mason, S.A., and Wattenberg, E.V. (2018). Anthropogenic contamination of tap water, beer, and sea salt. PLoS One *13*, e0194970. https://doi.org/10.1371/journal.pone.0194970.

21. Galloway, T.S., Cole, M., and Lewis, C. (2017). Interactions of microplastic debris throughout the marine ecosystem. Nat. Ecol. Evol. *1*, 116. https://doi.org/10.1038/s41559-017-0116.

22. Zarus, G.M., Muianga, C., Hunter, C.M., and Pappas, R.S. (2021). A review of data for quantifying human exposures to micro and nanoplastics and potential health risks. Sci. Total Environ. *756*, 144010. https://doi.org/10.1016/j.scitotenv.2020.144010.

23. Ragusa, A., Svelato, A., Santacroce, C., Catalano, P., Notarstefano, V., Carnevali, O., Papa, F., Rongioletti, M.C.A., Baiocco, F., Draghi, S., et al. (2021). Plasticenta: first evidence of microplastics in human placenta. Environ. Int. *146*, 106274. https://doi.org/10.1016/j.envint.2020.106274.

24. Breschi, A., Gingeras, T.R., and Guigó, R. (2017). Comparative transcriptomics in human and mouse. Nat. Rev. Genet. *18*, 425–440. https://doi.org/10.1038/nrg.2017.19.

25. Mörbe, U.M., Jørgensen, P.B., Fenton, T.M., von Burg, N., Riis, L.B., Spencer, J., and Agace, W.W. (2021). Human gut-associated lymphoid tissues (GALT); diversity, structure, and function. Mucosal immunol. *14*, 793–802. https://doi.org/10.1038/s41385-021-00389-4.

26. Garrett, N.L., Lalatsa, A., Uchegbu, I., Schätzlein, A., and Moger, J. (2012). Exploring uptake mechanisms of oral nanomedicines using multimodal nonlinear optical microscopy. J. Biophotonics *5*, 458–468. https://doi.org/10.1002/jbio.201200006.

27. Jani, P.U., Nomura, T., Yamashita, F., Takakura, Y., Florence, A.T., and Hashida, M. (1996). Biliary excretion of polystyrene microspheres with covalently linked FITC fluorescence after oral and parenteral administration to male Wistar rats. J. Drug Target. *4*, 87–93. https://doi.org/10.3109/10611869609046266.

28. Jin, Y., Lu, L., Tu, W., Luo, T., and Fu, Z. (2019). Impacts of polystyrene microplastic on the gut barrier, microbiota and metabolism of mice. Sci. Total Environ. *649*, 308–317. https://doi.org/10.1016/j.scitotenv.2018.08.353.

29. Lu, L., Wan, Z., Luo, T., Fu, Z., and Jin, Y. (2018). Polystyrene microplastics induce gut microbiota dysbiosis and hepatic lipid metabolism disorder in mice. Sci. Total Environ. *631–632*, 449–458. https://doi.org/10.1016/j.scitotenv.2018.03.051.

30. Deng, Y., Zhang, Y., Lemos, B., and Ren, H. (2017). Tissue accumulation of microplastics in mice and biomarker responses suggest widespread health risks of exposure. Sci. Rep. *7*, 46687. https://doi.org/10.1038/srep46687.

31. Wang, X., Zheng, H., Zhao, J., Luo, X., Wang, Z., and Xing, B. (2020). Photodegradation elevated the toxicity of polystyrene microplastics to grouper (Epinephelus moara) through disrupting hepatic lipid homeostasis. Environ. Sci. Technol. *54*, 6202–6212. https://doi.org/10.1021/acs.est.9b07016.

32. Gu, W., Liu, S., Chen, L., Liu, Y., Gu, C., Ren, H.Q., and Wu, B. (2020). Single-cell RNA sequencing reveals size-dependent effects of polystyrene microplastics on immune and secretory cell populations from zebrafish intestines. Environ. Sci. Technol. *54*, 3417–3427. https://doi.org/10.1021/acs.est.9b06386.

33. Luo, T., Wang, C., Pan, Z., Jin, C., Fu, Z., and Jin, Y. (2019). Maternal polystyrene microplastic exposure during gestation and lactation altered metabolic homeostasis in the dams and their F1 and F2 offspring. Environ. Sci. Technol. *53*, 10978–10992. https://doi.org/10.1021/acs.est.9b03191.

34. Deng, Y., Yan, Z., Shen, R., Wang, M., Huang, Y., Ren, H., Zhang, Y., and Lemos, B. (2020). Microplastics release phthalate esters and cause aggravated adverse effects in the mouse gut. Environ. Int. *143*, 105916. https://doi.org/10.1016/j.envint.2020.105916.

35. Reece, J.C., Vardaxis, N.J., Marshall, J.A., Crowe, S.M., and Cameron, P.U. (2001). Uptake of HIV and latex particles by fresh and cultured dendritic cells and monocytes. Immunol. Cell Biol. *79*, 255–263. https://doi.org/10.1046/j.1440-1711.2001.01011.x.

36. Yong, C.Q.Y., Valiyaveettil, S., and Tang, B.L. (2020). Toxicity of microplastics and nanoplastics in mammalian systems. Int. J. Environ. Res. Public Health *17*, 1509. https://doi.org/10.3390/ijerph17051509.

37. Kubes, P., and Jenne, C. (2018). Immune responses in the liver. Annu. Rev. Immunol. *36*, 247–277. https://doi.org/10.1146/annurev-immunol-051116-052415.

38. Parkin, J., and Cohen, B. (2001). An overview of the immune system. Lancet *357*, 1777–1789. https://doi.org/10.1016/S0140-6736(00)04904-7.

39. Heymann, F., and Tacke, F. (2016). Immunology in the liver–from homeostasis to disease. Nat. Rev. Gastroenterol. Hepatol. *13*, 88–110. https://doi.org/10.1038/nrgastro.2015.200.

40. Lewis, S.M., Williams, A., and Eisenbarth, S.C. (2019). Structure and function of the immune system in the spleen. Sci. Immunol. *4*, eaau6085. https://doi.org/10.1126/sciimmunol.aau6085.

41. Kanchanawong, P., and Calderwood, D.A. (2023). Organization, dynamics and mechanoregulation of integrin-mediated cell-ECM adhesions. Nat. Rev. Mol. Cell Biol. *24*, 142–161. https://doi.org/10.1038/s41580-022-00531-5.

42. Kalappurakkal, J.M., Anilkumar, A.A., Patra, C., van Zanten, T.S., Sheetz, M.P., Mayor, S., and Mayor, S. (2019). Integrin mechano-chemical signaling generates plasma membrane nanodomains that promote cell spreading. Cell *177*, 1738–1756.e23. https://doi.org/10.1016/j.cell.2019.04.037.

43. Humphries, J.D., Chastney, M.R., Askari, J.A., and Humphries, M.J. (2019). Signal transduction via integrin adhesion complexes. Curr. Opin. Cell Biol. *56*, 14–21. https://doi.org/10.1016/j.ceb.2018.08.004.

44. Simpson, B.W., and Trent, M.S. (2019). Pushing the envelope: LPS modifications and their consequences. Nat. Rev. Microbiol. *17*, 403–416. https://doi.org/10.1038/s41579-019-0201-x.

45. Roberts, N.J., Jr. (2020). Diverse and unexpected roles of human monocytes/macrophages in the immune response to Influenza virus. Viruses *12*, 379. https://doi.org/10.3390/v12040379.

46. Netea, M.G., Joosten, L.A., Latz, E., Mills, K.H., Natoli, G., Stunnenberg, H.G., O'Neill, L.A., and Xavier, R.J. (2016). Trained immunity: A program of innate immune memory in health and disease. Science *352*, aaf1098. https://doi.org/10.1126/science.aaf1098.

47. Boettner, B., and Van Aelst, L. (2009). Control of cell adhesion dynamics by Rap1 signaling. Curr. Opin. Cell Biol. *21*, 684–693. https://doi.org/10.1016/j.ceb.2009.06.004.

48. Li, K., and Underhill, D.M. (2020). C-type lectin receptors in phagocytosis. Curr. Top. Microbiol. Immunol. *429*, 1–18. https://doi.org/10.1007/82_2020_198.

49. Dey, R., Ji, K., Liu, Z., and Chen, L. (2009). A cytokine-cytokine interaction in the assembly of higher-order structure and activation of the interleukine-3:receptor complex. PLoS One *4*, e5188. https://doi.org/10.1371/journal.pone.0005188.

50. Joseph-Silverstein, J., and Silverstein, R.L. (1998). Cell adhesion molecules: an overview. Cancer Invest. *16*, 176–182. https://doi.org/10.3109/07357909809050034.

51. Takeda, K., and Akira, S. (2015). Toll-like receptors. Curr. Protoc. Immunol. *109*, 14.12.1–14.12.10. https://doi.org/10.1002/0471142735.im1412s109.

52. Amatya, N., Garg, A.V., and Gaffen, S.L. (2017). IL-17 Signaling: The Yin and the Yang. Trends Immunol. *38*, 310–322. https://doi.org/10.1016/j.it.2017.01.006.

53. Kayagaki, N., Warming, S., Lamkanfi, M., Vande Walle, L., Louie, S., Dong, J., Newton, K., Qu, Y., Liu, J., Heldens, S., et al. (2011). Non-canonical inflammasome activation targets caspase-11. Nature *479*, 117–121. https://doi.org/10.1038/nature10558.

54. Levental, K.R., Yu, H., Kass, L., Lakins, J.N., Egeblad, M., Erler, J.T., Fong, S.F.T., Csiszar, K., Giaccia, A., Weninger, W., et al. (2009). Matrix crosslinking forces tumor progression by enhancing integrin signaling. Cell *139*, 891–906. https://doi.org/10.1016/j.cell.2009.10.027.

55. Keely, P.J. (2011). Mechanisms by which the extracellular matrix and integrin signaling act to regulate the switch between tumor suppression and tumor promotion. J. Mammary Gland Biol. Neoplasia *16*, 205–219. https://doi.org/10.1007/s10911-011-9226-0.

56. Zhang, M., Yang, H., Wan, L., Wang, Z., Wang, H., Ge, C., Liu, Y., Hao, Y., Zhang, D., Shi, G., et al. (2020). Single-cell transcriptomic architecture and intercellular crosstalk of human intrahepatic cholangiocarcinoma. J. Hepatol. *73*, 1118–1130. https://doi.org/10.1016/j.jhep.2020.05.039.

57. Cai, X., Wang, J., Wang, J., Zhou, Q., Yang, B., He, Q., and Weng, Q. (2020). Intercellular crosstalk of hepatic stellate cells in liver fibrosis: New insights into therapy. Pharmacol. Res. *155*, 104720. https://doi.org/10.1016/j.phrs.2020.104720.

58. Weckmann, A.L., and Alcocer-Varela, J. (1996). Cytokine inhibitors in autoimmune disease. Semin. Arthritis Rheum. *26*, 539–557. https://doi.org/10.1016/s0049-0172(96)80042-4.

59. Pacheco, P., White, D., and Sulchek, T. (2013). Effects of microparticle size and Fc density on macrophage phagocytosis. PLoS One *8*, e60989. https://doi.org/10.1371/journal.pone.0060989.

60. Sun, F., Liao, Y., Qu, X., Xiao, X., Hou, S., Chen, Z., Huang, H., Li, P., and Fu, S. (2020). Hepatic DNAJB9 drives anabolic biasing to reduce steatosis and obesity. Cell Rep. *30*, 1835–1847.e9. https://doi.org/10.1016/j.celrep.2020.01.043.

61. Kim, D., Langmead, B., and Salzberg, S.L. (2015). HISAT: a fast spliced aligner with low memory requirements. Nat. Methods *12*, 357–360. https://doi.org/10.1038/nmeth.3317.

62. Li, B., and Dewey, C.N. (2011). RSEM: accurate transcript quantification from RNA-Seq data with or without a reference genome. BMC Bioinformatics *12*, 323. https://doi.org/10.1186/1471-2105-12-323.

63. Love, M.I., Huber, W., and Anders, S. (2014). Moderated estimation of fold change and dispersion for RNA-seq data with DESeq2. Genome Biol. *15*, 550. https://doi.org/10.1186/s13059-014-0550-8.

64. Wang, L., Feng, Z., Wang, X., Wang, X., and Zhang, X. (2010). DEGseq: an R package for identifying differentially expressed genes from RNA-seq data. Bioinformatics *26*, 136–138. https://doi.org/10.1093/bioinformatics/btp612.

65. Robinson, M.D., McCarthy, D.J., and Smyth, G.K. (2010). edgeR: a Bioconductor package for differential expression analysis of digital gene expression data. Bioinformatics *26*, 139–140. https://doi.org/10.1093/bioinformatics/btp616.

66. Xie, C., Mao, X., Huang, J., Ding, Y., Wu, J., Dong, S., Kong, L., Gao, G., Li, C.Y., and Wei, L. (2011). KOBAS 2.0: a web server for annotation and identification of enriched pathways and diseases. Nucleic Acids Res. *39*, W316–W322. https://doi.org/10.1093/nar/gkr483.

67. Luo, G., Zhao, L., Xu, X., Qin, Y., Huang, L., Su, Y., Zheng, W., and Yan, Q. (2019). Integrated dual RNA-seq and dual iTRAQ of infected tissue reveals the functions of a diguanylate cyclase gene of Pseudomonas plecoglossicida in host-pathogen interactions with Epinephelus coioides. Fish Shellfish Immunol. *95*, 481–490. https://doi.org/10.1016/j.fsi.2019.11.008.

68. Szklarczyk, D., Franceschini, A., Wyder, S., Forslund, K., Heller, D., Huerta-Cepas, J., Simonovic, M., Roth, A., Santos, A., Tsafou, K.P., et al. (2015). STRING v10: protein-protein interaction networks, integrated over the tree of life. Nucleic Acids Res. *43*, D447–D452. https://doi.org/10.1093/nar/gku1003.

69. Layssol-Lamour, C., Lavabre, T., Braun, J.P., Trumel, C., and Bourgès-Abella, N. (2019). The effects of storage at 4°C and 20°C on the hemograms of C57BL/6 mice and Wistar rats using the IDEXX ProCyte Dx and blood smear evaluations. Vet. Clin. Pathol. *48*, 652–667. https://doi.org/10.1111/vcp.12784.

STAR★METHODS

KEY RESOURCES TABLE

REAGENT or RESOURCE	SOURCE	IDENTIFIER
Chemicals, peptides, and recombinant proteins		
MPs	Base Line Chrom Tech Research Centre	Cat#7-3-0500
LPS	Sigma	Cat#L2630
Collagenase Type IV	Sigma	Cat#C5138
OCT	Sakura	Cat#4583
HBSS	Corning	Cat#21-022-CVR
$CaCl_2$	Solarbio	Cat#C8370
Penicillin/Streptomycin(P/S)	Solarbio	Cat#P1400
Primocin	InvivoGen	Cat#ant-pm-2
EGTA	Amresco	Cat#0732
Gelatin	Amresco	Cat#9764
HEPES	Amresco	Cat#0511
TRIzol	Life Technologies	Cat#15596018
DNase I	TaKara	Cat#2270A
B27	Thermo	Cat#17504044
Triton-X100	Thermo	Cat#85111
SDS	Thermo	Cat#28312
BCA	Thermo	Cat#23227
Urea	Merck	Cat#U5378
Critical commercial assays		
Annexin V-mCherry Apoptosis Detection Kit	Beyotime Biotechnology	Cat#C1069M
FastKing RT Kit (With gDNase)	TianGen	Cat#KR116-02
2X qPCR MasterMix-Low Rox	Abm	Cat#MasterMix-LR
Ribo-Zero Gold kit	Illumina	Cat#RS-123-2201
TNF ELISA Set	BD	Cat#555268
IL-6 ELISA Set	BD	Cat#555240
Deposited data		
MP-hepatic-gene sets	This paper	Harvard Dataverse https://doi.org/10.7910/DVN/QVSYWC
MP-spleen-gene sets	This paper	Harvard Dataverse https://doi.org/10.7910/DVN/QVSYWC
Statistical table of comparison results	This paper	Harvard Dataverse https://doi.org/10.7910/DVN/QVSYWC
Experimental models: Organisms/strains		
Mouse: C57BL/6J	Vital River Laboratory	Custom-ordered
Oligonucleotides		
Primers for quantitative RT-PCR, see Table S1	This paper	N/A
Software and algorithms		
FlowJo	BD Biosciences	http://www.flowjo.com
Image J	NIH	https://imagej.net/ImageJ
Adobe Illustrator CC 2018	Adobe	https://www.adobe.com
GraphPad Prism 8	GraphPad software	http://www.graphpad.com

RESOURCE AVAILABILITY

Lead contact

Further information and requests for resources and reagents should be directed to and will be fulfilled by the lead contact, Jiaqi Hou (houjiaqi0325@163.com).

Materials availability

This study did not generate new unique reagents.

Data and code availability

This study generated 20 unique datasets, and analytical results are all available in the Harvard Dataverse. Harvard Dataverse, V1, UNF: 6: SbUM+zW0vd+gPmSmFC1iQg= [fileUNF] (https://doi.org/10.7910/DVN/QVSYWC). Deposited data sets are listed in in the key resources table. This study did not generate any code. Any additional information required to reanalyze the data reported in this paper is available from the lead contact upon request.

EXPERIMENTAL MODEL AND STUDY PARTICIPANT DETAILS

Animal and MPs treatment

All the animal husbandry and experimental procedures were in strict accordance with the guidelines approved by the Institutional Animal Care and Use Committee (IACUC) of Tsinghua University. All mice were housed in a pathogen-free environment with *ad libitum* access to food and water, under controlled temperature conditions of 25±1°C on a 12-hour light/dark cycle. Wild-type (WT) C57BL/6J mice were procured from Vital River Laboratory.

In this study, we employed polyethylene plastic, a commonly utilized material in the field of biohazard research on MPs.[28–30,32,33] The polystyrene microsphere particles with a diameter of 5 μm, labeled with fluorescein isothiocyanate (FITC), were utilized as the MP treatment (7-3-0500, Base Line Chrom Tech Research Centre, Tianjin, China). Male mice at four weeks old were weighed and randomly divided into four groups based on comparable mean body weights. Of the 4 groups (n=5∼6 for each), 2 groups of control mice (CON) drank normal water and the other 2 groups of MP-exposed mice (MPs) drank water with a concentration of 10 μg/mL MPs (about 8.12×10^{11} particles/mL). Mice exposed to MPs were subjected to a 6-week exposure period. Subsequently, both control and treated mice underwent a standard 6-hour food withdrawal protocol at approximately 3:00 p.m. for sample collection.

METHOD DETAILS

Mice immune challenge

To elicit an immune response, LPS (Sigma-Aldrich, Saint Louis, MO, USA) was administered via intraperitoneal injection at a dose of 2 μg per g body weight in a volume of 200 μL.[48] Tissue samples from the liver and spleen as well as serum were collected four hours post-injection. Blood was collected 12 hours after the LPS injection to measure immune cell levels.

Histological analysis

For liver frozen sections, liver samples were promptly fixed in Optimal Cutting Temperature Compound (OCT) at -80°C. Then, the OCT-embedded tissues were cut into 8-mm-thick sections for fluorescence signal detection of FITC-labelled MPs. For hematoxylin and eosin (H&E) staining, liver samples were promptly fixed in 4% paraformaldehyde (PFA) after harvesting, dehydrated, and embedded. Paraffin-embedded tissues were cut into 6-μm-thick sections and stained with hematoxylin/eosin for cell morphology analysis.[60] Imaging data were processed and morphology analysis was performed using the ImageJ software (1.49V, NIH, Bethesda, MD, USA).

Primary hepatocyte isolation and FACS flow cytometry analysis

Mice were anesthetized with 250 mg/kg avertin, and the liver was perfused through the portal vein with 50 mL of warm (37°C) Hank's balanced salt solution (HBSS) buffer (Invitrogen, Carlsbad, CA, USA) supplemented with 1 mM ethylene glycol-bis (β-aminoethyl ether)-N, N, N′, N′-tetraacetic acid (EGTA) and 5 mM glucose (HBSS-EGTA) at a speed of 10-15 mL min^{-1} and then digested with 40 mL of collagenase IV (Sigma-Aldrich) prepared in HBSS buffer at the concentration of 0.25 mg/mL supplemented with 5 mM $CaCl_2$ and

5 mM glucose. Primary hepatocytes were suspended in HBSS-EGTA and sedimented at 500 rpm for 5 min. Cells were washed with HBSS and used in the flow cytometry assay. For measurement of MPs, the FITC signal was recorded by excitation at 494 nm and emission at 518 nm, to determine the distribution of cells interacting with MPs. Hepatocytes were incubated with 10 μg/mL of MPs for 10 min before FACS flow cytometry analysis and 0.1% Triton-X100 was used to remove membrane sticking MPs by incubation for 5 min before FACS flow cytometry analysis. For the measurement of cell apoptosis rate, 195 μL binding buffer and 5 μL of Annexin V-mCherry reagent (Annexin V-mCherry Apoptosis Detection Kit C1069M, Beyotime Biotechnology, Shanghai, China) were used to incubate hepatocyte at 20°C-25°C for 10-20 min, the mCherry signal was recorded by excitation at 587 nm and emission at 610 nm to determine the distribution of apoptotic cells.

Quantitative reverse transcribed polymerase chain reaction (qRT-PCR)

Total RNA was extracted using TRIzol reagent (Invitrogen) according to the manufacturer's recommendations. The mRNAs were reverse transcribed using the FastKing RT Kit (KR116; Tiangen, Beijing, China). Quantitative PCR was performed using the EvaGreen Mastermix on an Applied Biosystems StepOne or Vii7 Real-Time PCR System (Applied Biosystems, Foster City, CA, USA). Duplicate runs of each sample were normalized to *18S rRNA* to determine the relative gene expression levels.[60]

RNA extraction and library preparation

Total RNA was extracted from frozen tissues using TRIzol reagent (Invitrogen) according to the manufacturer's instructions. RNA samples were treated with DNase I (TaKara Bio Inc., Kusatsu, Shiga, Japan). A total of 500 ng RNA was used for library preparation with the TruSeq Stranded Total RNA with Ribo-Zero Gold kit (RS-123-2201; Illumina, San Diego, CA, USA). Then, the RNA quality was determined with a 2100 Bioanalyzer (Agilent Technologies, Santa Clare, USA) and quantified using the ND-2000 spectrometer (NanoDrop Technologies, Wilmington, DE, USA). Only high-quality RNA samples (OD260/280=1.8~2.2, OD260/230≥2.0, RIN≥6.5, 28S:18S≥1.0, >1 μg) were used to construct the sequencing library.

The RNA-seq transcriptome library was prepared following the TruSeq™ RNA sample preparation kit (Illumina) using 1 μg of total RNA. The raw paired-end reads were trimmed, and quality controlled using SeqPrep (https://github.com/jstjohn/SeqPrep) and Sickle (https://github.com/najoshi/sickle) with default parameters. Then, clean reads were separately aligned to the reference genome with orientation mode using HISAT2 (http://ccb.jhu.edu/software/hisat2/index.shtml).[61]

Differential gene expression analysis and functional enrichment

To identify DEGs between two different samples, the expression level of each transcript was calculated according to the transcripts per million reads (TPM) method. RSEM (http://deweylab.biostat.wisc.edu/rsem/)[62] was used to quantify gene abundance. Basically, differential expression analysis was performed using the DESeq2[63]/DEGseq[64]/EdgeR[65] with P-value ≤ 0.05, DEGs with |log2FC|>1 and P-value ≤ 0.05 (DESeq2 or EdgeR) /P-value ≤ 0.001(DEGseq) were considered to be significantly DEGs. In addition, functional-enrichment analyses, including GO and KEGG analyses, were performed to identify which DEGs were significantly enriched in GO terms and metabolic pathways at a Bonferroni-corrected P-value ≤ 0.05 compared with the whole-transcriptome background. GO functional enrichment and KEGG pathway analyses were performed using Goatools (https://github.com/tanghaibao/Goatools) and KOBAS (http://kobas.cbi.pku.edu.cn/home.do).[66]

Serum extraction and proteomic analysis

Total protein was extracted from serum using a urea lysis buffer (7 M urea, 2 M thiourea, and 1% sodium dodecyl sulfate) with a protease inhibitor. Protein concentration was measured with a bicinchoninic acid (BCA) Protein Assay Kit (Pierce, Thermo Fisher Scientific Inc., Waltham, MA, USA). Following reduction, cysteine alkylation, and digestion, the samples were labeled with iTRAQ Reagents (4390812; Applied Biosystems) according to the manufacturer's instructions. After desalting with a C18 solid-phase extraction cartridge, peptides were used for Nano Liquid Chromatography–tandem Mass Spectrometry (LC-MS/MS) analysis.[67] The RAW data files were analyzed using ProteomeDiscoverer Version 2.2 (Thermo Fisher Scientific Inc.) against the Mus musculus database (http://asia.ensembl.org/Mus_musculus/Info/Index, Assembly Version GRCm38, 67856s). Proteins expressed were identified as belonging to the serum proteome in this study. The thresholds of the fold change (>1.2 or <0.83) and P-value<0.05 were used to identify DEPs.

Annotation of all identified proteins was performed using GO (http://www.blast2go.com/b2ghome; http://geneontology.org/) and KEGG pathway (http://www.genome.jp/kegg/). DEPs were further used for GO and KEGG enrichment analysis. Protein-protein interaction analysis was performed using the String v10.5 database.[68]

Hematological analysis

Blood (100 μL) was collected from the fundus vein of mice using a capillary diameter of 0.5 mm and immediately placed in an anticoagulant vessel and oscillated to avoid coagulation.[69] Blood-related parameters were obtained by Procyte Dx analysis using the IDexx Procyte Dx* Hematology Analyzer (IDexx Laboratories Inc., Westbrook, ME, USA).

Serum cytokine measurement

For tumor necrosis factor-α (TNF-α) and Interleukin 6 (IL-6) measurements, blood was collected after 4 hs of LPS injection, centrifuged for 30 mins at 13,000 x g, 4°C to remove blood cells and debris, and measured by mouse TNF ELISA Set (BD Biosciences, Cat#555268), mouse IL-6 ELISA Set (BD Biosciences, Cat#555240), according to the manufacturer's instructions.

QUANTIFICATION AND STATISTICAL ANALYSIS

All data are reported as the mean ± Standard Error of Mean (SEM). Imaging data were processed with ImageJ (1.49V; NIH, Bethesda, MD, USA) and were plotted with GraphPad Prism 8.0 (GraphPad Software Inc., San Diego, CA, USA) and Adobe Illustrator CS6 (Adobe Inc., San Jose, CA, USA). Group differences were analyzed using the two-sided Student's t-test, and differences with P -value <0.05 were considered significant.